# Compact monopolar electrochemical stack designs using electrode arrays or corrugated electrodes

Rajaei, H.; Haverkort, J. W.

**DOI**
10.1016/j.electacta.2019.135470

**Publication date**
2020

**Document Version**
Final published version

**Published in**
Electrochimica Acta

Electrochimica Acta 332 (2020) 135470

Contents lists available at ScienceDirect

Electrochimica Acta

journal homepage: www.elsevier.com/locate/electacta

# Compact monopolar electrochemical stack designs using electrode arrays or corrugated electrodes

H. Rajaei, J.W. Haverkort*

*Process & Energy Department, Delft University of Technology, Leeghwaterstraat 39, 2628 CB, Delft, the Netherlands*

ARTICLE INFO

*Article history:*
Received 26 July 2019
Received in revised form
22 November 2019
Accepted 8 December 2019
Available online 12 December 2019

*Keywords:*
Printed electrodes
Electrode architecture
Electrolysers
Redox flow batteries

ABSTRACT

A new compact electrode architecture with hollow pillar-shaped anodes and cathodes arranged in a 'checkerboard' pattern is analysed and shown to be equivalent to a particular arrangement of corrugated plate electrodes. Because all four sides of the flow channels are electrodes, this design takes up at least 1.5 to two times less volume compared to conventional 'sandwich'-type configurations. The assumption underlying this theoretical scaling is illustrated with a 3D-printed metal prototype for alkaline water electrolysis using natural convection. For mass-transfer-limited electrolysers, fuel cells, electrowinning cells, and flow-batteries, the expected volume savings easily increase to a factor three or more.



## 1. Introduction

Electrochemical processes are rapidly becoming more relevant as society electrifies under the pressure of the climate agreement and the availability of affordable renewable electricity. A combination of water electrolysers and hydrogen fuel cells, as well as flow batteries, are likely to become cost-effective means of storing large amounts of electricity. A first generation of mass-produced fuel-cell consumer cars will soon compete with battery electric vehicles and large-scale water electrolysis projects are picking up as an alternative to hydrogen from steam methane reforming [1]. Alkaline water electrolysis is presently the most mature and competitive means of producing green hydrogen and is performed in large-scale electrolysers, similar to those used in the chlor-alkali industry.

Most of the studies in the field of alkaline water electrolysis focus on the development of catalysts and suitable substrates for electrodes, see e.g. Refs. [1,2]. Much less attention is given to cell and electrode configurations. Metal 3D-printing has led to optimized flow fields, and tailored porous substrates, but not to large changes in the convectional stacked planar electrode configuration [3]. Most modern electrolysers use a zero-gap design with macroporous metal electrodes positioned directly adjacent to the separators. This requires bubbles to leave through flow-channels at the backside of the electrodes [4–6]. The next generation of alkaline water electrolysers may take advantage of thinner separators [7] or even membrane-less designs [8–11]. For flow batteries and fuel cells, many studies into the flow field and bipolar plate design are published, see e.g. Refs. [12,13]. Also here, membraneless designs show promise [14] leading to some of the highest power densities achieved [15].

Here we study a new electrode configuration, a top-view of which is shown in Fig. 2. The idea is similar to that proposed for 3D-microbatteries in Refs. [16,17], since developed into self-supported 3D electrode nano-arrays [18]. Here we investigate the advantages that similar array electrodes can have for electrolysers, fuel cells, electrowinning cells, and flow batteries. As an illustrative example we developed a prototype for alkaline water electrolysis. Finally, we show that a corrugated electrode configuration as shown in Fig. (6) combine the same benefits with ease of manufacturing.

Besides the simplicity associated with the few components involved, the main advantage is shown to be a significant reduction in volume. This compactness will be useful for mobile applications like electric vehicles and drones, as well as in portable electronic devices like mobile phones and laptops.

## 2. Theory

### 2.1. Scalings

Fig. 1 compares a repeating unit of the conventional 'sandwich'

* Corresponding author.
*E-mail address:* J.W.Haverkort@tudelft.nl (J.W. Haverkort).

https://doi.org/10.1016/j.electacta.2019.135470

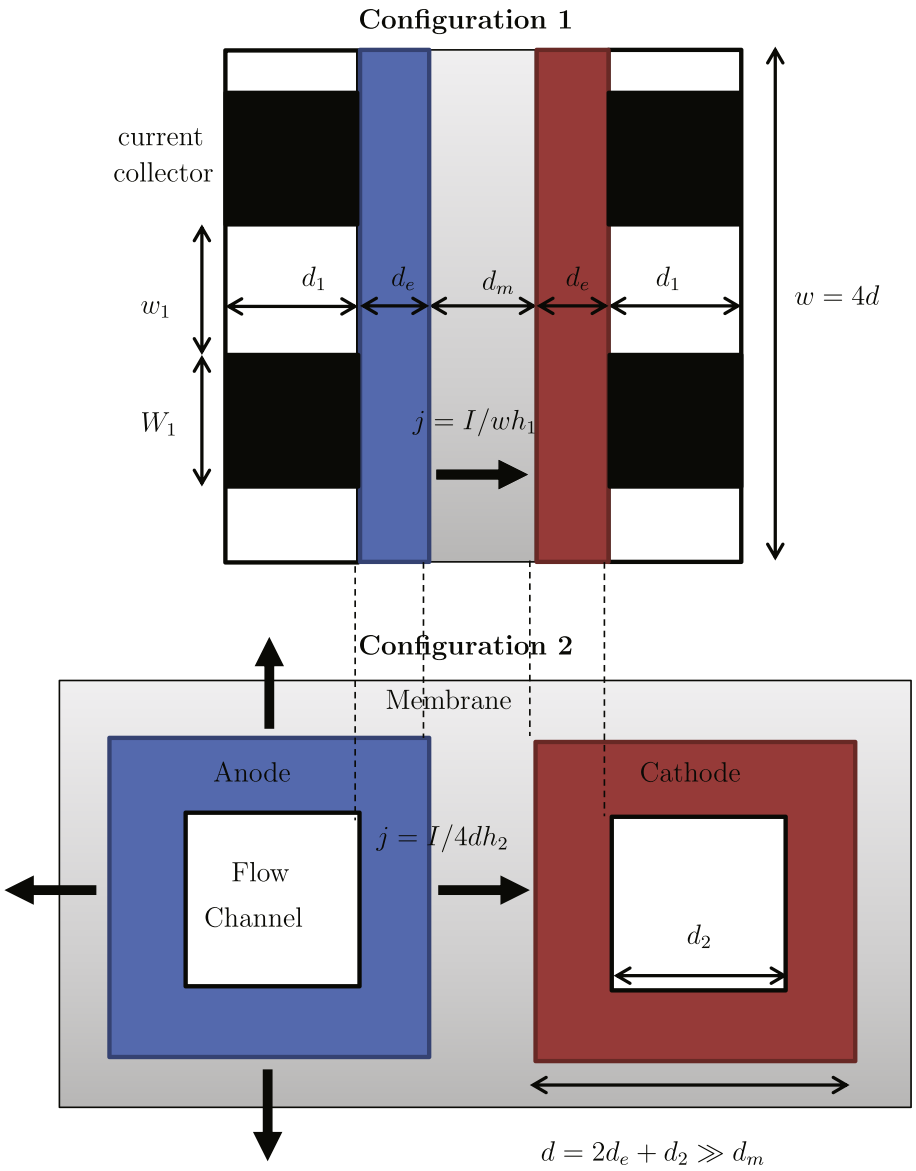


**Fig. 1.** A top-view schematic comparing the repeating units of configuration 1 (top) with configuration 2 (bottom). In a monopolar configuration 1, neighbouring repeating units are mirrored so that electrodes of equal polarity border.

configuration ("1") to that of an electrode array ("2"). We use the letters $h$, $w$ and $d$ to denote, height, widths, and depths, and a subscript 1 or 2 to denote the configuration. Our main goal in this section is to compare the material costs and volumes of both configurations. To make a fair comparison we have to be clear on what we assume to be equal in both configurations. A first obvious parameter is the current $I$ which, assuming equal selectivity or Faradaic efficiency, allows a comparison per amount of product. We will also consider equal electrode thickness $d_e$ and membrane thickness $d_m$ in both cases, although for simplicity we will often neglect these compared to the dimensions of the flow channels. In fuel cells, the combined thickness of the diffusion layer and membrane-electrode assembly (MEA) is of the order of 0.1 mm, while the flow channel thickness is of the order of 1 mm. In electrolysers, electrodes are typically of the order of 1 mm while the flow channels are of the order of 1 cm.

The assumption $d_m, d_e \ll d_2$ will ensure that in the array configuration 2, except for the negligibly small region near the corners, the current will be unidirectional in each membrane and electrode face. For equal current densities $j$ and membrane conductivity $\kappa_m$, this implies that the ohmic voltage drop $jd_m/\kappa_m$ over the membrane will be equal for both configurations. Similarly, the surface activation overpotentials will also be equal, resulting in an equal cell voltage and energy efficiency. A fair comparison will therefore have equal current densities in both configurations.

In the conventional configuration 1, the current will move in *one* single direction in case of a bipolar design, and *two* opposite directions in case of a monopolar set-up. In configuration 2, as illustrated with the arrows in Fig. 1, the current will be in *four* different directions, a different direction on each face of the electrode. At the same current density, equal current requires equal reactive areas:

$$\frac{I_1}{I_2} \approx \frac{\beta w h_1}{4 d h_2} = 1, \tag{1}$$

where $\beta \equiv w_1/(w_1 + W_1)$, assuming the electrode fraction $1 - \beta$ under the current collectors does not generate current. The

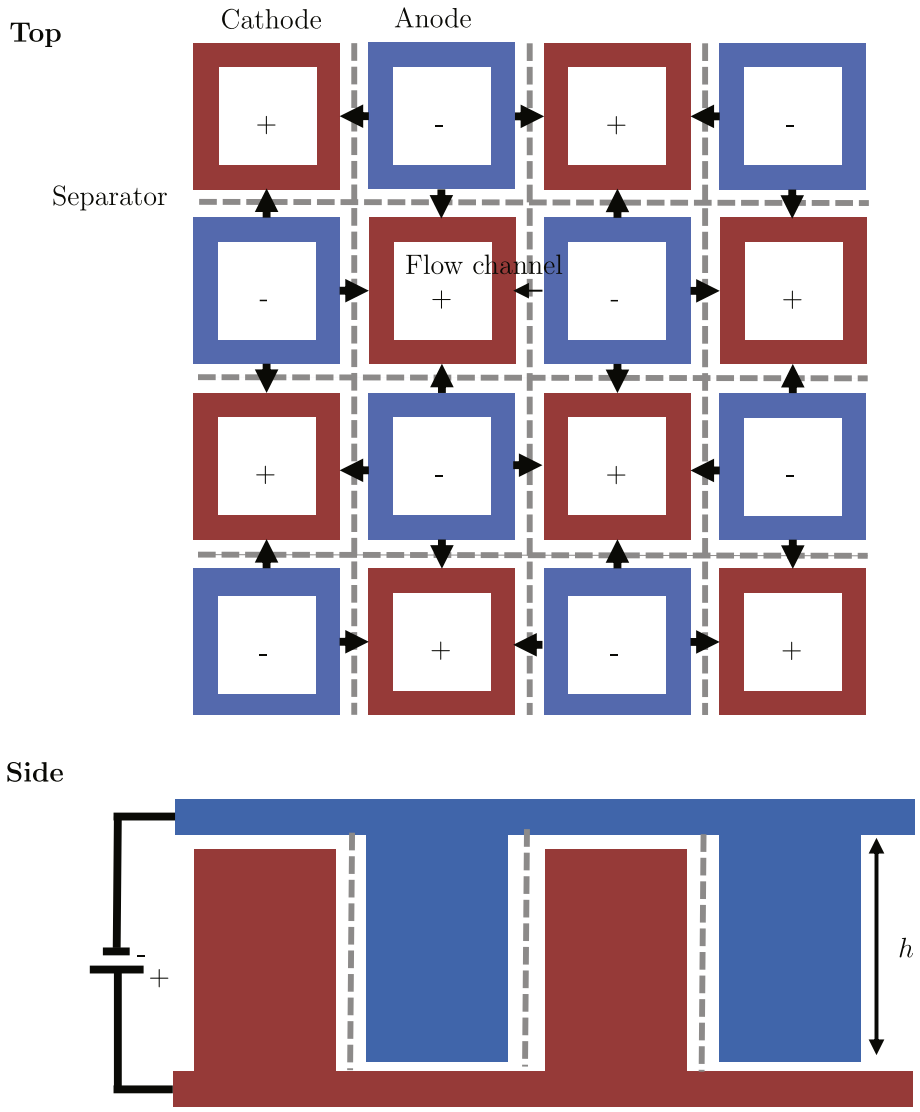


**Fig. 2.** A top-view (top) and side-view (bottom) of configuration 2.

assumption of equal reactive area immediately leads to the conclusion that, without the blocking effect of current collectors, a similar amount of electrode and membrane area is used in both configurations. The only potential materials savings are due to the absence of current collectors assumed in configuration 2, to which we will come back in section 2.2.

Comparing the volume $V$ (including current collectors) and flow-area $A$ (excluding current collectors) of the flow-channels gives:

$$\frac{V_1}{V_2}=\frac{wd_1}{d_2^2}\frac{h_1}{h_2}\approx\frac{4}{\beta}\frac{d_1}{d_2}, \tag{2}$$

$$\frac{A_1}{A_2}=\beta\frac{wd_1}{d_2^2}\approx 4\frac{d_1}{d_2}\frac{h_2}{h_1}. \tag{3}$$

In the final approximations we used Eq. (1) and neglected the membrane and electrode thickness to write $d_2\approx d$.

Minimizing the pressure drop at a desired flow-rate is often an important consideration for cost and energy efficiency. For systems with natural convection (section 2.3) or forced convection (2.4) this allows more compact designs or lower pumping costs, respectively. Therefore, for a fair comparison we require equal frictional channel pressure drop $\Delta p$ per unit volumetric flow rate $Q$. For fully-developed laminar flow this gives[1]

$$\frac{\Delta p_1/Q_1}{\Delta p_2/Q_2}=f\frac{d_2^2}{d_1^2}\frac{h_1}{h_2}\frac{A_2}{A_1}\approx\frac{f}{4}\frac{d_2^3}{d_1^3}\left(\frac{h_1}{h_2}\right)^2=1, \tag{4}$$

where $f\approx\frac{(1+\alpha)^2}{N}\left(0.42-0.3\left(\frac{\alpha}{1+\alpha^2}\right)^{0.79}\right)$ is a function of the channel aspect ratio $\alpha\equiv Nd_1/w_1$. Here $N=1$ in case of a bipolar configuration and $N=2$ for a monopolar configuration in which the pressure drop attributable to configuration 1 is halved since the flow channel

[1] $\Delta p=2\mu\frac{f\mathrm{Re}}{N}\frac{Q/A}{D_h^2}h$ in terms of the dynamic viscosity μ, product of Reynolds number and friction factor $f\mathrm{Re}$, and hydraulic diameter $D_h\equiv\frac{2wNd}{w+Nd}=\frac{2Nd}{1+\alpha}$. The function $f\mathrm{Re}\equiv(f\mathrm{Re})_1/(f\mathrm{Re})_2$ was fitted to within 1.5% difference to the data in Table 42 of Ref. [19].

is shared with the neighbouring electrode.

For equal heights $h_1 = h_2$, Eq. (2) finally gives, using Eq. (4):

$$\frac{V_1}{V_2} \approx \frac{4^{2/3} f^{1/3}}{\beta}. \tag{5}$$

For a completely open flow channel in configuration 1 we have $\alpha = 0$ and $\beta = 1$, giving a volume-saving-factor $V_1/V_2 \approx 1.9$ compared to a bipolar and 1.5 compared to a monopolar configuration. Note that $d_1/d_2 \approx 0.47$ and 0.37, respectively in these cases. The design of configuration 2 is therefore more compact despite its significantly larger flow channels; due to its reduced width.

Since flow channels are never empty, these values can be considered a lower limit to the potential volume-savings. For example, for square flow channels, Eq. (5) with $\alpha = 1$ gives $V_1/V_2 \approx 2.5/\beta$ or $2/\beta$ comparing with a bipolar or monopolar design, respectively. These volume-saving factors may of course also be used to create more product in the same volume or, producing the same amount per unit volume, to operate at a lower current density resulting in an increase in efficiency.

### 2.2. Current collection

In the electrode array of Fig. 2, the prototype of Fig. 3, and the corrugated electrode implementation of Fig. 6, electrodes of equal polarity are connected electrically to give a parallel electrical circuit. Although such unipolar or monopolar designs are still being produced, most modern alkaline electrolyzers electrically connect anodes to neighbouring cathodes in a bipolar configuration. In the resulting series circuit the voltage increases throughout the stack. This is advantageous for reducing electronic ohmic losses but also poses significant design restrictions to avoid bypass currents, or leaking currents [20]. Another disadvantage is the production of oxygen and hydrogen close together, requiring additional space and material costs to ensure separation. The main disadvantage of the much simpler monopolar design is the conductive requirement on the electrodes and current collectors, since current has to be transported out of each cell separately in the transverse direction. Since often a lower current at a higher voltage is preferred, additional voltage conversion is typically required.

With current collection from $M = 1$ or 2 sides, the top and/or bottom, the vertical current density $j_M(h_M - x)/h_M$ in the electrodes decreases with the distance $x$ from the current collector, resulting in an average ohmic drop of roughly $\Delta V = \frac{j_M}{\sigma h_M^2}\int_0^{h_M}(h_M - x)x dx = j_M h_M/6\sigma$. Here $\sigma$ is the effective electrode conductivity, $j_M = I/4dd_eM = jh_2/d_eM$ with $4dd_e$ the area that the current traverses and $h_M = h/M$. Limiting $\Delta V$ to a maximum, to avoid current maldistributions, gives

$$h < M\sqrt{\frac{6\sigma d_e \Delta V}{j}} \tag{6}$$

With $j = 0.5$ A/cm$^2$, $d_e = 0.5$ mm, $\sigma = 10^7$ S/m representative of perforated nickel, $N = 2$, and $\Delta V = 0.1$ V we obtain $h \leq 1.5$ m. This illustrates that even with relatively thin metal electrodes it will be possible to do without additional current collectors, even at higher current densities. Macro-porous metallic electrodes with sufficient structural rigidity, come in the form of expanded meshes, perforated plates, metal foams, and sintered particulate electrodes and are already used in a variety of applications [21]. Woven and non-woven metallic fibres like metal paper, felts, wool or gauze, may also be used but may need additional support to provide the required structural integrity.

### 2.3. Gas-evolution

In many electrolyzers, gases are produced. Obviously in the electrosynthesis of gases like chlorine, chlorate, or fluorine, and water electrolysis for hydrogen production, but also in the electroextraction of metals like zinc and copper and the Hall-Héroult process for smelting aluminium.

Atmospheric electrolyzers for the production of hydrogen, chlorate [22] or fluorine [23] are often operated without a pump, using the natural convection induced by the gas bubbles to drive a liquid flow. This results in a particularly maintenance-free and cost-effective design. To obtain a liquid velocity that helps remove bubbles and improves mass transport [22], the flow channels of such air-lift or gas-lift reactors is typically one to several centimetres wide [22]. Additional space is sometimes allocated for separate 'downcomers', through which the flow recirculates. In bipolar chlorate or chlor-alkali electrolyzers each cell typically has its own downcomer, requiring even more space.

The more compact flow channels in configuration 2 will carry the same amount of gas as in configuration 1. For an open flow channel, configuration 1 has a $A_1/A_2 \approx V_1/V_2 \approx 1.5$ to 2 times larger flow area per unit current when monopolar or bipolar, respectively. Per unit flow area there will thus be at least 1.5 to 2 times the volume of bubbles injected into the flow channel of configuration 2, resulting in larger gas fractions, driving larger liquid flows. Together with the micro-streaming of a larger amount of bubbles, this will help removing bubbles sticking to the electrodes, and improve heat and mass transfer. We can therefore argue that at equal current densities, in these respects the performance of configuration 2 is likely to be superior to that of configuration 1.

Additionally, in electrolyzers, springs or other elastic elements typically occupy the flow channel, increasing the normalized friction factor $f$. The O-beam type of electrodes of Fig. 2 or the corrugated electrodes of Fig. 6 can themselves provide sufficient strength so that no additional structural elements are necessary inside the flow channels. This further increases the flow properties compared to configuration 2. These combined effects will likely allow for a significantly more compact design than predicted by Eq. (5).

### 2.4. Mass transfer limitations

Besides removal of heat and products, flow channels in fuel cells, redox flow batteries, electrolysers, or electrorefining cells often have the important task of supplying sufficient reactants. Especially at low concentration of reactants, the reaction may be limited by the diffusive transfer inside the flow channels. This results in a limiting current density, which cannot be increased by increasing the overpotential. Here we will consider this common situation, assuming fully developed velocity and concentration profiles, relevant for reaching a high degree of conversion of reactants.

As in section 2.1 we will require equal current densities in both configurations, to give similar membrane and electrode costs. This will require equal mass transfer coefficients, leading to,[2]

$$\frac{j_1}{j_2} = \frac{g}{2}\frac{d_2}{d_1} = 1, \tag{7}$$

where $g \approx 1.64$. Inserting Eq. (7) into Eq. (2) and Eq. (4) gives

[2] The mass transfer coefficient $k = \mathrm{Sh}\mathbb{D}/D_h$ in terms of the dimensionless Sherwood number Sh, diffusion coefficient $\mathbb{D}$, and the hydraulic diameter $D_h = \frac{2wd}{w+d} = \frac{2d}{1+\alpha}$, equating to $d_2$ for configuration 2. The function $g \equiv (1+\alpha)\mathrm{Sh}_1/\mathrm{Sh}_2$ was obtained using an anology with heat transfer from a fit (< 4% difference) of the Nusselt number data in Table 44 of Ref. [19].

$$\frac{V_1}{V_2} \approx \frac{3.3}{\beta} \quad \text{and} \quad \frac{h_1}{h_2} \approx \frac{1.5}{\sqrt{f}}. \tag{8}$$

So without current collectors ($\alpha = 0$, $\beta = 1$) the flow-channel volume of configuration 2 can be reduced by a factor 3.3 compared to configuration 1. A bipolar conventional design requires (with $f \approx 0.42$) a $h_1/h_2 \approx 2.3$ times higher channel. From Eq. (7) we have $d_1/d_2 = g/2 \approx 0.82$ so that the flow channels are less deep. However, from Eq. (1) $w/d_2 \approx 4h_2/\beta h_1 \approx 1.73$ so that configuration 1 has to be significantly wider than configuration 2 to obtain the same current.

The reason for this large volume reduction is that all four faces of the flow channel are reactive in configuration 2, instead of just a single face in the case of configuration 1. Note that for a monopolar design, using Eq. (8) with $f \approx 0.21$, the volume-saving $V_1/V_2 \approx h_1/h_2 \approx 3.3$ will be the same as for a bipolar configuration. The reason is that, by symmetry, there will be no flux midway the monopolar flow-channel, bringing no advantage in mass transport. The only improvement is in pressure drop, allowing width to be traded for additional height. Note that by using a serpentine flow field, cell height may effectively, always be traded for cell width.

Flow channels in fuel cells or redox flow batteries are often engraved in the bipolar plates, so that the ribs partially block the flow channels. An optimal 'land-to-channel-width ratio' $W_1/w_1 = \frac{1-\beta}{\beta}$ of the order unity or even larger [24] is typically used to given and as homogeneous as possible current distribution. Rigid metallic electrodes can replace both the functionality of current collection and provide structural integrity, while strongly reducing the required volume at the same time.

Mass transfer limited process are ubiquitous in industry: in organic and inorganic electrosynthesis, metal recovery, and process or waste water treatment [25]. Parallel plate electrolysers, stacked in filter-press type of reactors, are generally used for decontamination and water treatment [26]. Reduction of $CO_2$ in aqueous electrolytes allows integration with capture and ease of separation of gaseous products like CO, but poor mass transfer is sometimes considered inhibitive for using a parallel plate configuration [27]. An additional factor of 3.3 current per unit volume, at the same pressure drop, perhaps in combination with increased pressure, may aid this business case.

Applying 'turbulence promotors' even larger enhancement factors in the mass transfer rate can be obtained [28]. This typically however leads to similar increases in the pressure drop. An attractive feature of the enhancement found here this holds without an increase in pressure drop.

## 3. Prototype experiments

In order to illustrate some of the differences of array and planar electrodes, we designed and manufactured the two configurations for application to alkaline electrolysis, see Fig. 3. The electrodes ($h = 2$ cm, $d_e = 2$ mm, with a porosity $\varepsilon \approx 0.5$) were made with a metal 3D printer (Sisma Mysint 100 p.m.) from 316 L stainless steel. The 250 μm diamond-shaped pores slope 45° upwards from the separator to facilitate bubble removal. A $d_m = 0.5$ mm thick separator (Zirfon Perl, Agfa Co.) is folded between the electrodes as shown in Fig. 3.

The optimal electrode thickness $d_{e,\mathrm{opt}} \approx 4b\kappa\varepsilon/j$, with $\kappa \approx$ 55 S/m the electrolyte ionic conductivity and $b \approx$ 55 mV the Tafel slope and the optimal porosity $\varepsilon \approx 0.5$ for a particular electrode with straight non-tortuous pores, were chosen based on the energy efficiency analysis of Ref. [29]. At a current densities $j = 0.3$ A/cm$^2$ this gives an optimal thickness of 2 mm, which was used. We chose $d = 8$ mm, leaving $d_2 = 4$ mm wide flow channels, clearly violating the assumption $d \approx d_2$ used in the analysis above. This allowed to fit in a larger number of anodes (17) and cathodes (18) into the maximum dimensions allowed in the 3D printer. In calculating the current density, we excluded the electrode area not directly facing another electrode.

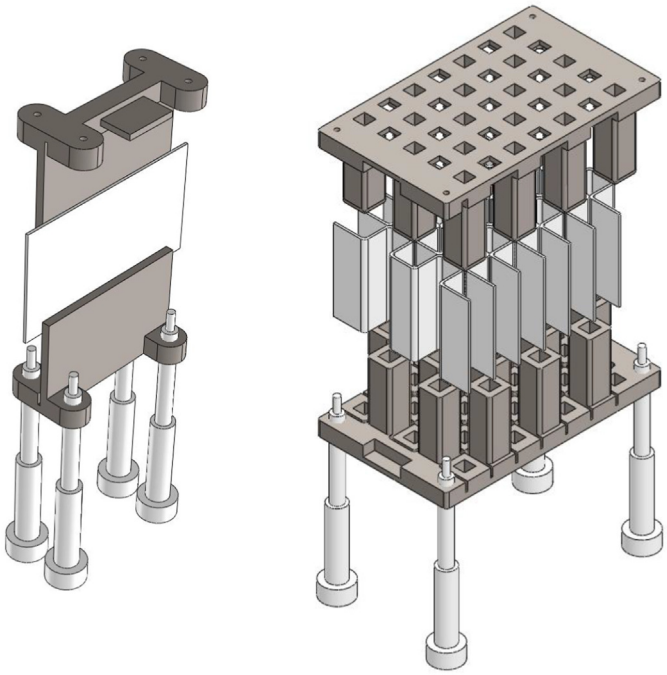

**Fig. 3.** A 3D rendering of the alkaline electrolysis prototypes created to compare a single cell of configuration 1 (left) with an array electrode version of configuration 2 (right).

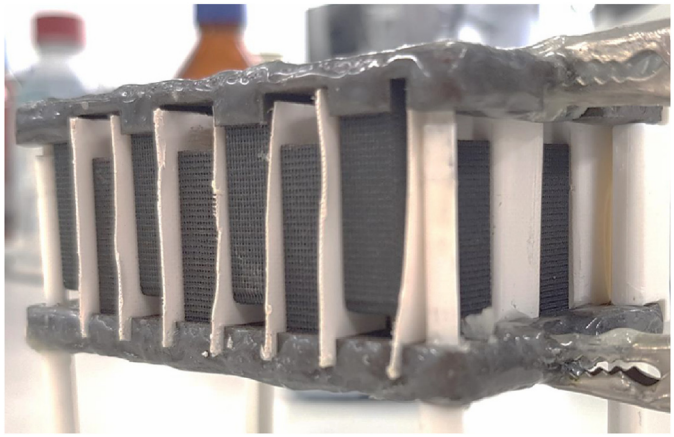

**Fig. 4.** A picture of the 3D-printed alkaline array electrolyser. Crocodile clamps for current collection, and an epoxy glue to avoid bubble formation of the top and bottom end-plates, can be seen.

Both prototypes were placed inside an open container filled with 30%$w$ KOH solution. The electrolyte was continuously pumped through a degassing ultrasound bath to avoid accumulation of bubbles and allowing a steady state current and voltage to be obtained.

Fig. 5 compares the polarization curves of the two configurations. The overpotential of about 0.5 V at 500 A/m$^2$ is relatively high because the electrode material, steel, is not an optimal catalyst for

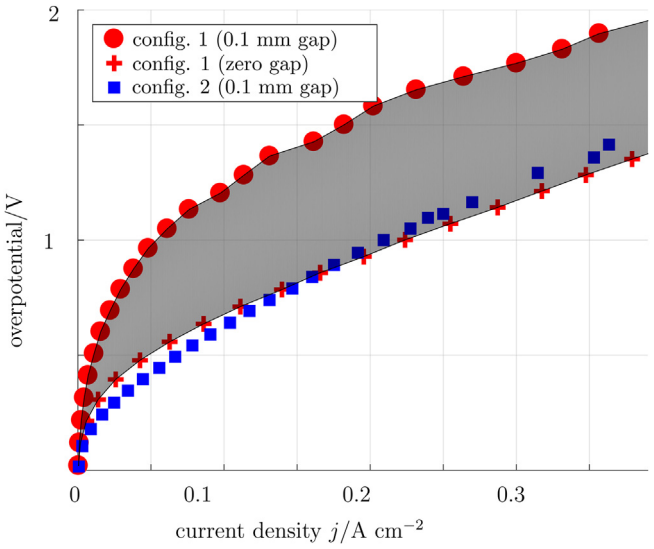


**Fig. 5.** The overpotential as a function of current density shows very similar results for configuration 1 (zero-gap, red crosses) and 2 (blue squares). Presumably due to the accumulation of an insulating bubble layer, the overpotential shoots up in configuration when, as in configuration 1, a 0.1 mm gap is introduced. (For interpretation of the references to colour in this figure legend, the reader is referred to the Web version of this article.)

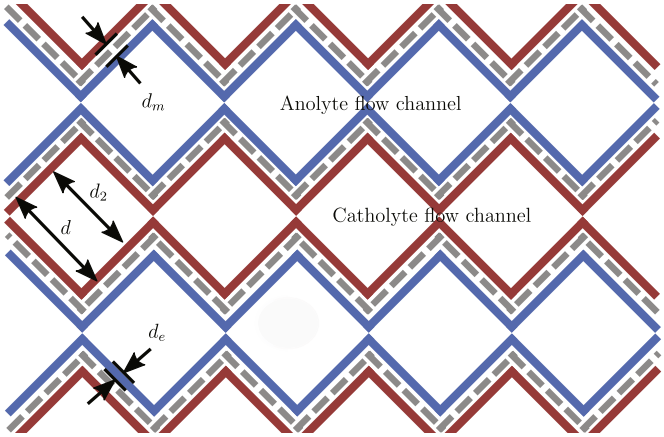


**Fig. 6.** A corrugated electrode and membrane configuration showing geometrical equivalence with the electrode array of Fig. 2 tilted by 45°. The topological change of connecting neighbouring electrodes of equal polarity greatly simplifies manufacturing while also allowing current collection from the sides. At the vertices between different flow channels additional current collectors can be placed or additional space for flow created. The flow direction is normal to the paper/screen. To enhance mass transfer inside thick porous electrodes, flowing one or both electrolyte streams in the horizontal direction may however also be considered. Finally, various shapes other than square flow channels can be created, including hexagonal and smoothly undulating nearly circular channels.

hydrogen or oxygen evolution.

To allow the separator to be folded in between the electrodes, a small 0.1 mm gap was left on both sides of the separator in configuration 2. Apart from a slightly higher slope at high current densities, characteristic of the larger distance between the electrodes, the performance of configuration 2 compares well with the zero-gap version of configuration 1. Introducing the same 0.1 mm gap in configuration 1, however, a strong increase in the overpotential was observed, likely due to bubbles accumulating in this gap [5]. Possibly due to the curvature in the folded separator, or the improved hydrodynamics, this strong effect of bubbles was not found in configuration 2.

The design of Figs. 3 and 4 with all anodes and all cathodes attached to separate end-plates, allowed for easy current collection. While we here allowed both gases to escape through the top end plate, separation can be easily established by closing the holes in the top current collector-plate in connection with the anodes, and providing a path for oxygen to leave from the sides, so that the pure hydrogen can be collected from the top. The advantages of the corrugated electrode design of Fig. 6 in terms of strength, additional current collection from the sides, ease of electrode manufacturing and allowing a true zero-gap will probably decide in favour of this configuration for large scale applications.

Importantly, the results of Eq. (5) tentatively confirm our central assumption that at equal current densities $j$ the losses are similar in both configurations.

## 4. Discussion and conclusions

We introduced an innovative electrode architecture in which each anode is surrounded by four cathodes, and vice versa. At equal current densities, the amount of electrode and membrane materials will be similar to that of a conventional configuration. The monopolar design avoids bypass currents and obviates the need for separate current collectors or bipolar plates by collecting products in separate flow channels. For equal pressure drops, these flow channels will be a factor 1.5 and 1.9 less voluminous than in a monopolar and bipolar conventional configurations, respectively. In gas-evolving electrolysers with natural convection this volume-saving factor will be even higher, or alternatively the performance with respect to mass transfer and bubble removal will be superior. For mass transfer-limited reactors, the volume savings are calculated to be at least a factor 3.3, owing to the fact that all four walls of the flow channels constitute reactive electrode area. We showed that these benefits of array electrodes can also be obtained by a simple stacking of corrugating planar electrodes and membranes. The increased compactness, simplicity, and ease of manufacturing are expected to greatly benefit scale-up and cost reductions of a variety of electrochemical flow reactors.

## Author contribution section

H. Rajaei: Methodology, Investigation, Writing, Visualization
J.W. Haverkort: Conceptualization, Methodology, Writing, Visualization, Supervision, Funding acquisition

## Acknowledgements

We thank P.I. van der Stigchel, J.C. Troost, K. Bani, R.G. Naber, and W.G. Scholts for their help in creating the prototype. We gratefully acknowledge funding support from Shell Global Solutions International B·V, Netherlands, under agreement number PT73368.

## References

[1] M. David, C. Ocampo-Martinez, R. Sánchez-Peña, Advances in alkaline water electrolyzers: a review, J. Energ. Stor. 23 (2019) 392–403.
[2] A.N. Colli, H.H. Girault, A. Battistel, Non-precious electrodes for practical alkaline water electrolysis, Materials 12 (2019) 1336.
[3] C.-Y. Lee, A.C. Taylor, A. Nattestad, S. Beirne, G.G. Wallace, 3d Printing for Electrocatalytic Applications, 2019. Joule.
[4] R.L. Costa, P.G. Grimes, Electolysis as Source of Hydrogen and Oxygen, Technical Report, Allis-Chalmers Mfg. Co., Milwaukee, 1967.
[5] V. Kienzlen, D. Haaf, W. Schnurnberger, Location of hydrogen gas evolution on perforated plate electrodes in zero gap cells, Int. J. Hydrogen Energy 19 (1994) 729–732.
[6] R. Phillips, C.W. Dunnill, Zero gap alkaline electrolysis cell design for renewable energy storage as hydrogen gas, RSC Adv. 6 (2016) 100643–100651.
[7] I. Vincent, A. Kruger, D. Bessarabov, Hydrogen Production by Water

Electrolysis with an Ultrathin Anion-Exchange Membrane (Aem), 2018.
[8] J.T. Davis, J. Qi, X. Fan, J.C. Bui, D.V. Esposito, Floating membraneless pv-electrolyzer based on buoyancy-driven product separation, Int. J. Hydrogen Energy 43 (2018) 1224–1238.
[9] D.V. Esposito, Membrane-coated Electrocatalysts an Alternative Approach to Achieving Stable and Tunable Electrocatalysis, 2017.
[10] M.I. Gillespie, F. Van der Merwe, R.J. Kriek, Performance evaluation of a membraneless divergent electrode-flow-through (deft) alkaline electrolyser based on optimisation of electrolytic flow and electrode gap, J. Power Sources 293 (2015) 228–235.
[11] S.M.H. Hashemi, P. Karnakov, P. Hadikhani, E. Chinello, S. Litvinov, C. Moser, P. Koumoutsakos, D. Psaltis, A versatile and membrane-less electrochemical reactor for the electrolysis of water and brine, Energy Environ. Sci. 12 (2019) 1592–1604, https://doi.org/10.1039/C9EE00219G.
[12] T. Wilberforce, Z. El Hassan, E. Ogungbemi, O. Ijaodola, F. Khatib, A. Durrant, J. Thompson, A. Baroutaji, A. Olabi, A comprehensive study of the effect of bipolar plate (bp) geometry design on the performance of proton exchange membrane (pem) fuel cells, Renew. Sustain. Energy Rev. 111 (2019) 236–260.
[13] X. Ke, J.M. Prahl, J.I.D. Alexander, J.S. Wainright, T.A. Zawodzinski, R.F. Savinell, Rechargeable redox flow batteries: flow fields, stacks and design considerations, Chem. Soc. Rev. 47 (2018) 8721–8743.
[14] M.O. Bamgbopa, S. Almheiri, H. Sun, Prospects of recently developed membraneless cell designs for redox flow batteries, Renew. Sustain. Energy Rev. 70 (2017) 506–518.
[15] M.E. Suss, K. Conforti, L. Gilson, C.R. Buie, M.Z. Bazant, Membraneless flow battery leveraging flow-through heterogeneous porous media for improved power density and reduced crossover, RSC Adv. 6 (2016) 100209–100213.
[16] R.W. Hart, H.S. White, B. Dunn, D.R. Rolison, 3-d microbatteries, Electr. Commun. 5 (2003) 120–123.
[17] J.W. Long, B. Dunn, D.R. Rolison, H.S. White, Three-dimensional battery architectures, Chem. Rev. 104 (2004) 4463–4492.
[18] J. Liu, D. Zhu, Y. Zheng, A. Vasileff, S.-Z. Qiao, Self-supported earth-abundant nanoarrays as efficient and robust electrocatalysts for energy-related reactions, ACS Catal. 8 (2018) 6707–6732.
[19] R. Shah, A. London, Advances in Heat Transfer, Laminar Forced Flow Convection in Ducts, Suppl, vol. 1, 1978.
[20] R. LeRoy, A. Stuart, Advanced unipolar electrolysis, Int. J. Hydrogen Energy 6 (1981) 589–599.
[21] L. Arenas, C.P. de León, F. Walsh, 3d porous metal electrodes: fabrication, characterisation and use, Curr. Opin. Electrochem. 16 (2019) 1–9, https://doi.org/10.1016/j.coelec.2019.02.002.
[22] P. Boissonneau, P. Byrne, An experimental investigation of bubble-induced free convection in a small electrochemical cell, J. Appl. Electrochem. 30 (2000) 767–775.
[23] J.S. Hur, C.B. Shin, H. Kim, Y.S. Kwon, Modeling of the trajectories of the hydrogen bubbles in a fluorine production cell, J. Electrochem. Soc. 150 (2003) D70–D78.
[24] Y. Kerkoub, A. Benzaoui, F. Haddad, Y.K. Ziari, Channel to rib width ratio influence with various flow field designs on performance of pem fuel cell, Energ. convers. manage. 174 (2018) 260–275.
[25] D. Pletcher, F.C. Walsh, Industrial Electrochemistry, Springer Science & Business Media, 2012.
[26] F. Walsh, L. Arenas, C.P. de León, Developments in plane parallel flow channel cells, Curr. Opin. Electrochem 16 (2019) 10–18, https://doi.org/10.1016/j.coelec.2019.02.006.
[27] J.-B. Vennekoetter, R. Sengpiel, M. Wessling, Beyond the catalyst: how electrode and reactor design determine the product spectrum during electrochemical $CO_2$ reduction, Chem. Eng. J. 364 (2019) 89–101.
[28] A.N. Colli, R. Toelzer, M.E.H. Bergmann, J.M. Bisang, Mass-transfer studies in an electrochemical reactor with a small interelectrode gap, Electrochim. Acta 100 (2013) 78–84.
[29] J.W. Haverkort, A theoretical analysis of the optimal electrode thickness and porosity, Electrochim. Acta 295 (2019) 846–860.